A Branch-and-Bound Algorithm for Globally Optimal Hand-Eye Calibration

Jan Heller Michal Havlena Tomas Pajdla
Czech Technical University, Faculty of Electrical Engineering,
Karlovo náměstí 13, Prague, Czech Republic
{hellej1,havlem1,pajdla}@cmp.felk.cvut.cz

Abstract

This paper introduces a novel solution to hand-eye calibration problem. It is the first method that uses camera measurements directly and at the same time requires neither prior knowledge of the external camera calibrations nor a known calibration device. Our algorithm uses branch-and-bound approach to minimize an objective function based on the epipolar constraint. Further, it employs Linear Programming to decide the bounding step of the algorithm. The presented technique is able to recover both the unknown rotation and translation simultaneously and the solution is guaranteed to be globally optimal with respect to the L_∞-norm.

1. Introduction

The need to relate measurements made by a camera to a different known coordinate system arises in many engineering applications. Historically, it appeared for the first time in the connection with cameras mounted on robotic systems. The problem is commonly known as *hand-eye calibration* and has been studied abundantly in the past. Early solution methods solved for rotational and translational parts separately [13, 14, 11, 2]. Such separation inevitably leads to propagation of the residual error of the estimated rotation into the translation estimation, so later on methods for simultaneous estimation of both rotation and translation appeared [7, 3, 15].

However, none of these methods work with camera measurements directly. They require prior knowledge of the external camera calibrations instead. Specifically, an objective function based on camera transformation matrices, rather that a more geometrically meaningful criteria based on the original camera measurements, is minimized in all of the algorithms.

Recently, Heller *et al*. [6] proposed a method for optimal estimation of the translational part from camera measurement. However, it still requires prior knowledge of the relative camera rotations and solves for rotation separately.

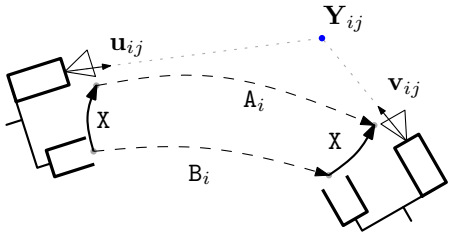

Figure 1: A gripper-camera rig motion.

In work by Seo *et al.* [10], the rotational part is solved optimally but all the translations are assumed to be zero.

In this paper we solve for rotation and translation simultaneously by minimizing an objective function based on the epipolar constraint without any prior knowledge of the external camera calibration. Our method is based on branch-and-bound search over the space of rotations presented in [4] and is guaranteed to converge to the optimum with respect to L_∞-norm.

First, we motivate the problem using a camera rigidly mounted on a robotic gripper. Next, we overview the branch-and-bound scheme and derive a feasibility test for the bounding step of the algorithm based on *Linear Programming* (LP). Finally, we validate the method experimentally using both synthetic and real world datasets.

2. Problem Formulation

Let's assume a camera has been rigidly mounted on a robot's gripper. To find hand-eye calibration is to determine a homogeneous transformation

$$\mathtt{X} = \begin{pmatrix} \mathtt{R}_\mathtt{X} & \mathbf{t}_\mathtt{X} \\ \mathbf{0}^\top & 1 \end{pmatrix},$$

such that rotation $\mathtt{R}_\mathtt{X} \in \mathrm{SO}(3) \subset \mathbb{R}^{3\times 3}$ and translation $\mathbf{t}_\mathtt{X} \in \mathbb{R}^3$ transform the coordinate system of the gripper to the coordinate system of the camera.

Now let's suppose that the gripper has been manipulated into $n+1$ positions resulting into n relative motions. These motions can be described by homogeneous transformations

$\mathtt{B}_i$, $i = 1, \ldots, n$ and are supposed to be known, *e.g.*, obtained from the robot's control software. The gripper's motions give rise to n relative camera transformations $\mathtt{A}_i$, which are related to $\mathtt{B}_i$ through the unknown transformation $\mathtt{X}$ as

$$\mathtt{A}_i\mathtt{X} = \mathtt{X}\mathtt{B}_i,$$

see Figure 1. This equation can be further decomposed to

$$\begin{aligned} \mathtt{R}_{\mathtt{A}_i}\mathtt{R}_\mathtt{X} &= \mathtt{R}_\mathtt{X}\mathtt{R}_{\mathtt{B}_i}, \\ \mathtt{R}_{\mathtt{A}_i}\mathbf{t}_\mathtt{X} + \mathbf{t}_{\mathtt{A}_i} &= \mathtt{R}_\mathtt{X}\mathbf{t}_{\mathtt{B}_i} + \mathbf{t}_\mathtt{X}, \end{aligned}$$

where $\mathtt{R}_{\mathtt{A}_i}, \mathtt{R}_{\mathtt{B}_i} \in \mathrm{SO}(3)$ and $\mathbf{t}_{\mathtt{A}_i}, \mathbf{t}_{\mathtt{B}_i} \in \mathbb{R}^3$. By substituting $\mathbf{t}'_\mathtt{X} = -\mathtt{R}_\mathtt{X}^\top \mathbf{t}_\mathtt{X}$ and isolating $\mathtt{R}_{\mathtt{A}_i}$ and $\mathbf{t}_{\mathtt{A}_i}$ respectively, we get

$$\mathtt{R}_{\mathtt{A}_i} = \mathtt{R}_\mathtt{X}\mathtt{R}_{\mathtt{B}_i}\mathtt{R}_\mathtt{X}^\top, \; \mathbf{t}_{\mathtt{A}_i} = \mathtt{R}_\mathtt{X}\left(\left(\mathtt{R}_{\mathtt{B}_i} - \mathtt{I}\right)\mathbf{t}'_\mathtt{X} + \mathbf{t}_{\mathtt{B}_i}\right).$$

Further suppose that in the i-th motion the camera measured m correspondences $\mathbf{u}_{ij} \leftrightarrow \mathbf{v}_{ij}$, $j = 1, \ldots, m$. Through the rest of the paper we will assume that the camera's internal calibration is known [5] and that $\mathbf{u}_{ij}, \mathbf{v}_{ij} \in \mathbb{R}^3$ are unit vectors representing the directions to scene points from the respective camera positions. Further, we will assume that the correspondences satisfy *the cheirality condition* [5], *i.e.*, that $\mathbf{u}_{ij}, \mathbf{v}_{ij}$ correspond to scene points $\mathbf{Y}_{ij} \in \mathbb{R}^3$ that lie in front of the cameras.

Let us consider an elementary fact from the geometry of stereo vision known as *the epipolar constraint* [5]. For camera motion $\mathtt{A}_i$ it states that if vectors $\mathbf{u}_{ij}$ and $\mathbf{v}_{ij}$ form a correspondence, $\mathbf{t}_{\mathtt{A}_i}$ lies in the plane containing the two vectors. Putting it into an equation,

$$e_{ij} = \angle([\mathbf{v}_{ij}]_\times \mathtt{R}_{\mathtt{A}_i}\mathbf{u}_{ij}, \mathbf{t}_{\mathtt{A}_i}) - \tfrac{\pi}{2} = 0,$$

where $[\cdot]_\times$ denotes the 3×3 skew symmetric matrix such that $\forall \mathbf{u}, \mathbf{v}\colon \; [\mathbf{u}]_\times \mathbf{v} = \mathbf{u} \times \mathbf{v}$. This will however not hold for noised measurements and so we can formulate hand-eye calibration as an optimization problem:

Problem 1

$$(\hat{\mathtt{R}}_\mathtt{X}, \hat{\mathbf{t}}'_\mathtt{X}) = \operatorname*{arg\,min}_{\mathtt{R}_\mathtt{X}, \mathbf{t}'_\mathtt{X}} \max_{i,j} \left| \angle([\mathbf{v}_{ij}]_\times \mathtt{R}_{\mathtt{A}_i}\mathbf{u}_{ij}, \mathbf{t}_{\mathtt{A}_i}) - \tfrac{\pi}{2} \right|.$$

This problem can be also seen as L_∞-norm minimization of vector $\mathbf{e} = (|e_{11}|, \ldots, |e_{ij}|)$ with the residual error $\epsilon = \|\mathbf{e}\|_\infty$. After solving Problem 1, the optimal translation is determined as $\hat{\mathbf{t}}_\mathtt{X} = -\hat{\mathtt{R}}_\mathtt{X}\hat{\mathbf{t}}'_\mathtt{X}$. This substitution may seem superfluous, however, it will allow us to proof the correctness of the branch-and-bound algorithm later.

3. Branch and Bound

In order to solve Problem 1 we employ branch-and-bound optimization to search over the space of all rotations presented in [4]. We represent rotations using the angle-axis parametrization, where all rotations can be represented by vectors in the closed ball of radius π, $\mathbb{B}_\pi = \{\boldsymbol{\alpha} : \|\boldsymbol{\alpha}\| \leq \pi\}$. Let $D_\sigma \subset \mathbb{B}_\pi$ be a cubic block in the rotation space with side length 2σ. Let's consider Problem 1 restricted to D_σ:

Problem 2

$$(\hat{\mathtt{R}}_\mathtt{X}, \hat{\mathbf{t}}'_\mathtt{X}) = \operatorname*{arg\,min}_{\mathtt{R}_\mathtt{X} \in D_\sigma, \mathbf{t}'_\mathtt{X}} \max_{i,j} \left| \angle([\mathbf{v}_{ij}]_\times \mathtt{R}_{\mathtt{A}_i}\mathbf{u}_{ij}, \mathbf{t}_{\mathtt{A}_i}) - \tfrac{\pi}{2} \right|.$$

Here $\mathtt{R}_\mathtt{X} \in D_\sigma$ stands for all rotations represented by block D_σ. The structure of brand-and-bound is as follows.

1. Obtain initial an estimate of $\epsilon_{\min}$ for the optimal solution of Problem 1.
2. Divide up the space of rotations into cubic blocks D_σ^j and repeat the following steps.
   (a) For each block D_σ^j test whether there exists a solution to the restricted Problem 2 on D_σ^j having the residual error smaller than $\epsilon_{\min}$. This test can be formulated as a *feasibility test*, see Section 5.
   (b) If the answer to the test is no, throw the block away.
   (c) Otherwise, evaluate the residual error ϵ for some rotation from block D_σ^j. If $\epsilon < \epsilon_{\min}$ then update the value $\epsilon_{\min} \leftarrow \epsilon$. Subdivide D_σ^j into eight cubic sub-blocks and continue to (a).

The iteration loop is terminated when the size of the block σ reaches a sufficiently small size $\sigma_{\min}$.

Note that although Problem 1 has 6 degrees of freedom, we search only over the tree dimensional space of rotations. By limiting rotations in angle-axis parametrization to D_σ we are able to decide the feasibility test for Problem 2 effectively and optimally using LP. The LP solution also provides $\mathbf{t}'_\mathtt{X}$ needed to compute the residual error in step (c) and thus we have no need to search over the space of translations.

4. The Geometry of the Space of Rotations

In this section we establish the relation between matrix and angle-axis parameterizations of rotations and provide necessary lemmas for the proof of correctness of the hand-eye feasibility test.

Let $\boldsymbol{\alpha} \in \mathbb{B}_\pi$, then $\boldsymbol{\alpha}$ represents the rotation about axis $\boldsymbol{\alpha}/\|\boldsymbol{\alpha}\|$ by angle $\|\boldsymbol{\alpha}\|$. The corresponding matrix parametrization $\mathtt{R} \in \mathrm{SO}(3)$ can be obtained as

$$\mathtt{R} = \exp[\boldsymbol{\alpha}]_\times = \mathtt{I} + \frac{[\boldsymbol{\alpha}]_\times \sin\|\boldsymbol{\alpha}\|}{\|\boldsymbol{\alpha}\|} + \frac{[\boldsymbol{\alpha}]_\times^2 (1 - \cos\|\boldsymbol{\alpha}\|)}{\|\boldsymbol{\alpha}\|}.$$

This relation is also known as *Rodrigues' formula*. The inverse map is given by

$$[\boldsymbol{\alpha}]_\times = \log \mathtt{R} = \frac{1}{\sin\left(\arccos\frac{\mathrm{trace}(\mathtt{R})-1}{2}\right)}\left(\mathtt{R} - \mathtt{R}^\top\right).$$

Now we can precisely define $\mathtt{R} \in D \subset \mathbb{B}_\pi$ as the shorthand for $\mathtt{R} \in \left\{\mathtt{R}' \in \mathrm{SO}(3) \colon \exists \boldsymbol{\alpha} \in D \text{ such that } \mathtt{R}' = \exp[\boldsymbol{\alpha}]_\times\right\}$.

For $\mathtt{R}_1, \mathtt{R}_2 \in \mathrm{SO}(3)$ we define the distance $d_\angle(\mathtt{R}_1, \mathtt{R}_2)$ as the angle θ of the rotation $\mathtt{R}_1^\top \mathtt{R}_2$, such that $0 \leq \theta \leq \pi$.

The following four lemmas are from [4].

Lemma 1 *Let* $\mathtt{R}_1, \mathtt{R}_2 \in \mathrm{SO}(3)$. *Then for* $\forall\, \mathbf{v} \in \mathbb{R}^3$

$$\angle(\mathtt{R}_1\mathbf{v}, \mathtt{R}_2\mathbf{v}) \leq d_\angle(\mathtt{R}_1, \mathtt{R}_2).$$

Lemma 2 *Let* $\boldsymbol{\alpha}_1, \boldsymbol{\alpha}_2 \in \mathbb{B}_\pi$ *and* $\mathtt{R}_1, \mathtt{R}_2 \in \mathrm{SO}(3)$ *such that* $\mathtt{R}_1 = \exp[\boldsymbol{\alpha}_1]_\times$ *and* $\mathtt{R}_2 = \exp[\boldsymbol{\alpha}_2]_\times$. *Then*

$$d_\angle(\mathtt{R}_1, \mathtt{R}_2) \leq \|\boldsymbol{\alpha}_1 - \boldsymbol{\alpha}_2\|.$$

Lemma 3 *Let* $\bar{\mathtt{R}}_\mathtt{X}$ *be the rotation represented by the center of a cube* $D_\sigma \subset \mathbb{B}_\pi$ *and* $\mathtt{R}_\mathtt{X} \in D_\sigma$. *Then for* $\forall\, \mathbf{v} \in \mathbb{R}^3$

$$\angle(\bar{\mathtt{R}}_\mathtt{X}\mathbf{v}, \mathtt{R}_\mathtt{X}\mathbf{v}) \leq \sqrt{3}\sigma.$$

Lemma 4 *Let* $\mathbf{u}, \mathbf{v}, \mathbf{w} \in \mathbb{R}^3$ *be unit vectors determining a spherical triangle on a unit sphere and the edges be arcs of lengths* u, v, *and* w *respectively. Let* α, β *be the angles at* $\mathbf{v}$ *and* $\mathbf{w}$ *respectively. It follows that if* β *is a right angle then* $\sin\alpha = \sin v / \sin w$.

The following two lemmas are from [10].

Lemma 5 *Let* $\mathtt{R}_\mathtt{X} \in \mathrm{SO}(3)$ *and* $\boldsymbol{\beta} \in \mathbb{B}_\pi$. *Then*

$$\log \mathtt{R}_\mathtt{X} [\boldsymbol{\beta}]_\times \mathtt{R}_\mathtt{X}^\top = [\mathtt{R}_\mathtt{X}\boldsymbol{\beta}]_\times.$$

Lemma 6 *Let* $\bar{\mathtt{R}}_\mathtt{X}$ *be the rotation represented by the center of a cube* $D_\sigma \subset \mathbb{B}_\pi$, $\boldsymbol{\beta} \in \mathbb{B}_\pi$. *Then for* $\forall\, \mathtt{R}_\mathtt{X} \in D_\sigma$

$$\|\bar{\mathtt{R}}_\mathtt{X}\boldsymbol{\beta} - \mathtt{R}_\mathtt{X}\boldsymbol{\beta}\| \leq 2\|\boldsymbol{\beta}\| \sin(\sqrt{3}\sigma/2).$$

Let us prove two more lemmas here.

Lemma 7 *Let* $\bar{\mathtt{R}}_\mathtt{X}$ *be the rotation represented by the center of a cube* $D_\sigma \subset \mathbb{B}_\pi$, $\boldsymbol{\beta} \in \mathbb{B}_\pi$. *Let* $\mathtt{R}_\mathtt{X} \in D_\sigma$ *and* $\mathtt{R}_\mathtt{A} = \mathtt{R}_\mathtt{X} \exp[\boldsymbol{\beta}]_\times \mathtt{R}_\mathtt{X}^\top$, $\bar{\mathtt{R}}_\mathtt{A} = \bar{\mathtt{R}}_\mathtt{X} \exp[\boldsymbol{\beta}]_\times \bar{\mathtt{R}}_\mathtt{X}^\top$. *Then for* $\forall\, \mathbf{u} \in \mathbb{R}^3$

$$\angle(\bar{\mathtt{R}}_\mathtt{A}\mathbf{u}, \mathtt{R}_\mathtt{A}\mathbf{u}) \leq 2\|\boldsymbol{\beta}\| \sin\left(\sqrt{3}\sigma/2\right).$$

Proof. Note where Lemmas 1, 5, 2 and 6 were used, respectively.

$$\begin{aligned}\angle(\bar{\mathtt{R}}_\mathtt{A}\mathbf{u}, \mathtt{R}_\mathtt{A}\mathbf{u}) &\leq d_\angle(\bar{\mathtt{R}}_\mathtt{A}, \mathtt{R}_\mathtt{A}) \\ &= d_\angle(\exp[\bar{\mathtt{R}}_\mathtt{X}\boldsymbol{\beta}]_\times, \exp[\mathtt{R}_\mathtt{X}\boldsymbol{\beta}]_\times) \\ &\leq \|\bar{\mathtt{R}}_\mathtt{X}\boldsymbol{\beta} - \mathtt{R}_\mathtt{X}\boldsymbol{\beta}\| \\ &\leq 2\|\boldsymbol{\beta}\| \sin(\sqrt{3}\sigma/2).\end{aligned}$$

□

Lemma 8 *Let* $\bar{\mathtt{R}}_\mathtt{X}$ *be the rotation represented by the center of a cube* $D_\sigma \subset \mathbb{B}_\pi$, $\boldsymbol{\beta} \in \mathbb{B}_\pi$ *and* $\mathbf{u}, \mathbf{v} \in \mathbb{R}^3$. *Let* $\mathtt{R}_\mathtt{X} \in D_\sigma$ *and* $\mathtt{R}_\mathtt{A} = \mathtt{R}_\mathtt{X} \exp[\boldsymbol{\beta}]_\times \mathtt{R}_\mathtt{X}^\top$, $\bar{\mathtt{R}}_\mathtt{A} = \bar{\mathtt{R}}_\mathtt{X} \exp[\boldsymbol{\beta}]_\times \bar{\mathtt{R}}_\mathtt{X}^\top$. *Then if* $\angle(\pm\mathbf{v}, \bar{\mathtt{R}}_\mathtt{A}\mathbf{u}) > 2\|\boldsymbol{\beta}\| \sin(\sqrt{3}\sigma/2)$, *the following inequality holds*

$$\angle([\mathbf{v}]_\times \bar{\mathtt{R}}_\mathtt{A}\mathbf{u}, [\mathbf{v}]_\times \mathtt{R}_\mathtt{A}\mathbf{u}) \leq \arcsin\left(\frac{\sin(2\|\boldsymbol{\beta}\| \sin(\sqrt{3}\sigma/2))}{\sqrt{1-(\mathbf{v}^\top \bar{\mathtt{R}}_\mathtt{A}\mathbf{u})^2}}\right).$$

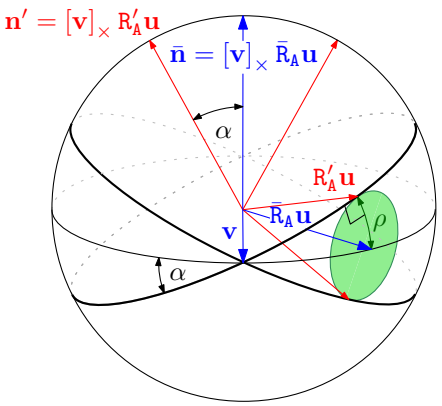

Figure 2: Illustration of the proof of Lemma 8.

Proof. We know from Lemma 7 that for every $\mathtt{R}_\mathtt{X} \in D_\sigma$ and $\mathbf{u} \in \mathbb{R}^3$ the angle $\angle(\bar{\mathtt{R}}_\mathtt{A}\mathbf{u}, \mathtt{R}_\mathtt{A}\mathbf{u})$ is limited by $\rho = 2\|\boldsymbol{\beta}\| \sin(\sqrt{3}\sigma/2)$, see Figure 2. Let $\mathbf{v} \in \mathbb{R}^3$ such that $\angle(\pm\mathbf{v}, \bar{\mathtt{R}}_\mathtt{A}\mathbf{u}) > \rho$, *i.e.*, vectors $\pm\mathbf{v}$ do not lie in the cone C determined by vector $\bar{\mathtt{R}}_\mathtt{A}\mathbf{u}$ and radius ρ. Now let's consider the geometrical relation between vectors $\bar{\mathbf{n}} = [\mathbf{v}]_\times \bar{\mathtt{R}}_\mathtt{A}\mathbf{u}$ and $\mathbf{n} = [\mathbf{v}]_\times \mathtt{R}_\mathtt{A}\mathbf{u}$. It is an elementary geometrical fact, that if $\mathbf{v}$, $\mathtt{R}_\mathtt{A}\mathbf{u}$ and $\bar{\mathtt{R}}_\mathtt{A}\mathbf{u}$ are coplanar vectors, then $\angle(\bar{\mathbf{n}}, \mathbf{n}) = 0$. Let $\mathtt{R}'_\mathtt{X} \in D_\sigma$ be a rotation such that the plane determined by vector $\mathbf{n}' = [\mathbf{v}]_\times \mathtt{R}'_\mathtt{A}\mathbf{u}$ is tangential to the cone C. Trivially, $\forall \mathtt{R}_\mathtt{X} \in D_\sigma$: $\angle(\bar{\mathbf{n}}, \mathbf{n}) \leq \angle(\bar{\mathbf{n}}, \mathbf{n}')$. Now the angle $\alpha = \angle(\bar{\mathbf{n}}, \mathbf{n}')$ can be determined. By using Lemma 4 on vectors $\mathbf{v}$, $\mathtt{R}'_\mathtt{A}\mathbf{u}$ and $\bar{\mathtt{R}}_\mathtt{A}\mathbf{u}$ we get

$$\sin\alpha = \frac{\sin\angle([\mathbf{v}]_\times \bar{\mathtt{R}}_\mathtt{A}\mathbf{u}, [\mathbf{v}]_\times \mathtt{R}_\mathtt{A}\mathbf{u})}{\sin\angle(\mathbf{v}, \bar{\mathtt{R}}_\mathtt{A}\mathbf{u})} = \frac{\sin\rho}{\sin\arccos \mathbf{v}^\top \bar{\mathtt{R}}_\mathtt{A}\mathbf{u}}.$$

From this follows that for $\forall \mathtt{R}_\mathtt{X} \in D_\sigma$

$$\angle(\bar{\mathbf{n}}, \mathbf{n}) \leq \alpha = \arcsin \frac{\sin\rho}{\sqrt{1-(\mathbf{v}^\top \bar{\mathtt{R}}_\mathtt{A}\mathbf{u})^2}}.$$

□

5. Feasibility Test for Hand-Eye Calibration

In this section the feasibility test for branch-and-bound is formulated.

First, let us introduce a few more shorthands

$$\begin{aligned}\bar{\mathtt{R}}_{\mathtt{A}_i} &= \bar{\mathtt{R}}_\mathtt{X}\mathtt{R}_{\mathtt{B}_i}\bar{\mathtt{R}}_\mathtt{X}^\top, \ \bar{\mathbf{t}}_{\mathtt{A}_i} = \bar{\mathtt{R}}_\mathtt{X}\left((\mathtt{R}_{\mathtt{B}_i} - \mathtt{I})\,\mathbf{t}'_\mathtt{X} + \mathbf{t}_{\mathtt{B}_i}\right), \\ \hat{\mathtt{R}}_{\mathtt{A}_i} &= \hat{\mathtt{R}}_\mathtt{X}\mathtt{R}_{\mathtt{B}_i}\hat{\mathtt{R}}_\mathtt{X}^\top, \ \hat{\mathbf{t}}_{\mathtt{A}_i} = \hat{\mathtt{R}}_\mathtt{X}\left((\mathtt{R}_{\mathtt{B}_i} - \mathtt{I})\,\mathbf{t}'_\mathtt{X} + \mathbf{t}_{\mathtt{B}_i}\right).\end{aligned}$$

5.1. Feasibility Test Formulation

The following is Problem 2 written as a feasibility test.

Problem 3

$$\begin{aligned}&\textit{Given}\ \ D_\sigma, \epsilon_{\min} \\ &\textit{do there exist}\ \ \mathtt{R}_\mathtt{X} \in D_\sigma, \mathbf{t}'_\mathtt{X} \\ &\quad\textit{subject to}\ \ \angle([\mathbf{v}_{ij}]_\times \mathtt{R}_{\mathtt{A}_i}\mathbf{u}_{ij}, \mathbf{t}_{\mathtt{A}_i}) \leq \tfrac{\pi}{2} + \epsilon_{\min} \\ &\qquad\qquad \angle(-[\mathbf{v}_{ij}]_\times \mathtt{R}_{\mathtt{A}_i}\mathbf{u}_{ij}, \mathbf{t}_{\mathtt{A}_i}) \leq \tfrac{\pi}{2} + \epsilon_{\min} \\ &\qquad\textit{for}\ \ i = 1, \ldots, n,\ \ j = 1, \ldots, m\ ?\end{aligned}$$

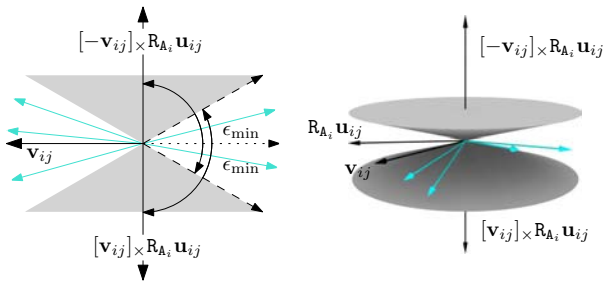

Figure 3: Geometrical interpretation of the conic constraint imposed by the correspondence $\mathbf{u}_{ij} \leftrightarrow \mathbf{v}_{ij}$. The cyan vectors show examples of the possible configurations of $\mathbf{t}_{\mathtt{A}_i}$.

Note how the absolute value was eliminated by splitting the constraint in two. A correspondence $\mathbf{u}_{ij} \leftrightarrow \mathbf{v}_{ij}$ imposes a *conic constraint*, see Figure 3, *i.e.*, the respective $\mathbf{t}_{\mathtt{A}_i}$ has to lie outside of the cone determined by axis $[\mathbf{v}_{ij}]_\times \mathtt{R}_{\mathtt{A}_i}\mathbf{u}_{ij}$ and aperture $\pi - 2\epsilon_{\min}$. Unfortunately, Problem 3 is not convex and thus not easy to solve. Let $\bar{\mathtt{R}}_{\mathtt{X}}$ be the rotation represented by the center of cube D_σ and let $\boldsymbol{\beta}_i \in \mathbb{B}_\pi$ such that $\exp[\boldsymbol{\beta}_i]_\times = \mathtt{R}_{\mathtt{B}_i}$. Now, let us consider a slightly weaker problem:

Problem 4

$$\begin{aligned}
&\textit{Given } D_\sigma, \epsilon_{\min}, \bar{\mathtt{R}}_{\mathtt{X}} \\
&\textit{does there exist } \mathbf{t}'_{\mathtt{X}} \\
&\textit{subject to } \angle([\mathbf{v}_{ij}]_\times \bar{\mathtt{R}}_{\mathtt{A}_i}\mathbf{u}_{ij}, \bar{\mathbf{t}}_{\mathtt{A}_i}) \le \tfrac{\pi}{2} + \epsilon_{\min} + \gamma_{ij} \\
&\qquad \angle(-[\mathbf{v}_{ij}]_\times \bar{\mathtt{R}}_{\mathtt{A}_i}\mathbf{u}_{ij}, \bar{\mathbf{t}}_{\mathtt{A}_i}) \le \tfrac{\pi}{2} + \epsilon_{\min} + \gamma_{ij} \\
&\textit{for } i = 1, \ldots, n,\ j = 1, \ldots, m \\
&\textit{such that } \angle(\pm\mathbf{v}_{ij}, \bar{\mathtt{R}}_{\mathtt{A}}\mathbf{u}_{ij}) > 2\,\|\boldsymbol{\beta}_i\| \sin(\sqrt{3}\sigma/2)\ ?
\end{aligned}$$

Lemma 9 describes the relation between Problems 3 and 4 and provides exact formulations of bounds γ_{ij} .

Lemma 9 *Relation between Problems 3 and 4.*

1. *If Problem 3 is feasible so is Problem 4.*
2. *If Problem 3 is infeasible, then D_σ may be split into subdomains $D^j_{\sigma'}$ of sufficiently small half-side length σ' such that Problem 4 is infeasible in every $D^j_{\sigma'}$.*

Proof. First we prove the first part of the lemma. Let's suppose that $\hat{\mathtt{R}}_{\mathtt{X}} \in D_\sigma$ and $\mathbf{t}'_{\mathtt{X}} \in \mathbb{R}^3$ constitute a feasible solution for Problem 3. We show that $\hat{\mathtt{R}}_{\mathtt{X}}$, $\mathbf{t}'_{\mathtt{X}}$ constitute a solution for Problem 4 as well. Let us consider a correspondence $\mathbf{u}_{ij} \leftrightarrow \mathbf{v}_{ij}$. If $\angle(\pm\mathbf{v}_{ij}, \bar{\mathtt{R}}_{\mathtt{A}}\mathbf{u}_{ij}) \le 2\,\|\boldsymbol{\beta}_i\| \sin(\sqrt{3}\sigma/2)$—one of the preconditions of Lemma 8 is not fulfilled—we cannot easily decide about the constraint imposed by the correspondence. If, on the other hand, this condition is met, we can write the following inequality

$$\begin{aligned}
&\angle([\mathbf{v}_{ij}]_\times \bar{\mathtt{R}}_{\mathtt{A}_i}\mathbf{u}_{ij}, \bar{\mathbf{t}}_{\mathtt{A}_i}) && (1)\\
\le\ &\angle([\mathbf{v}_{ij}]_\times \bar{\mathtt{R}}_{\mathtt{A}_i}\mathbf{u}_{ij}, [\mathbf{v}_{ij}]_\times \hat{\mathtt{R}}_{\mathtt{A}_i}\mathbf{u}_{ij}) && (2)\\
&+\angle([\mathbf{v}_{ij}]_\times \hat{\mathtt{R}}_{\mathtt{A}_i}\mathbf{u}_{ij}, \hat{\mathbf{t}}_{\mathtt{A}_i}) + \angle(\hat{\mathbf{t}}_{\mathtt{A}_i}, \bar{\mathbf{t}}_{\mathtt{A}_i}) \\
\le\ &\angle([\mathbf{v}_{ij}]_\times \bar{\mathtt{R}}_{\mathtt{A}_i}\mathbf{u}_{ij}, [\mathbf{v}_{ij}]_\times \hat{\mathtt{R}}_{\mathtt{A}_i}\mathbf{u}_{ij}) && (3)\\
&+\tfrac{\pi}{2} + \epsilon_{\min} + \angle\left(\hat{\mathtt{R}}_{\mathtt{X}}((\mathtt{R}_{\mathtt{B}_i} - \mathtt{I})\mathbf{t}'_{\mathtt{X}} + \mathbf{t}_{\mathtt{B}_i}),\right. \\
&\qquad\qquad \left.\bar{\mathtt{R}}_{\mathtt{X}}((\mathtt{R}_{\mathtt{B}_i} - \mathtt{I})\mathbf{t}'_{\mathtt{X}} + \mathbf{t}_{\mathtt{B}_i})\right) \\
\le\ &\angle([\mathbf{v}_{ij}]_\times \bar{\mathtt{R}}_{\mathtt{A}_i}\mathbf{u}_{ij}, [\mathbf{v}_{ij}]_\times \hat{\mathtt{R}}_{\mathtt{A}_i}\mathbf{u}_{ij}) && (4)\\
&\qquad +\tfrac{\pi}{2} + \epsilon_{\min} + \sqrt{3}\sigma \\
\le\ &\arcsin\left(\frac{\sin\left(2\|\boldsymbol{\beta}_i\| \sin\left(\sqrt{3}\sigma/2\right)\right)}{\sqrt{1-\left(\mathbf{v}_{ij}^\top \bar{\mathtt{R}}_{\mathtt{A}_i}\mathbf{u}_{ij}\right)^2}}\right) && (5)\\
&\qquad +\tfrac{\pi}{2} + \epsilon_{\min} + \sqrt{3}\sigma
\end{aligned}$$

To elaborate, we get from line 1 to line 2 by twice applying the triangle inequality, to line 3 using the presumption that $\hat{\mathtt{R}}_{\mathtt{X}}$, $\mathbf{t}'_{\mathtt{X}}$ constitute a solution to Problem 3, to line 4 using Lemma 3, and finally to line 5 using Lemma 8. Now, line 5 gives us value of the bound γ_{ij} as

$$\gamma_{ij} = \arcsin\left(\frac{\sin\left(2\|\boldsymbol{\beta}_i\| \sin\left(\sqrt{3}\sigma/2\right)\right)}{\sqrt{1-\left(\mathbf{v}_{ij}^\top \bar{\mathtt{R}}_{\mathtt{A}_i}\mathbf{u}_{ij}\right)^2}}\right) + \sqrt{3}\sigma.$$

The proof of the second inequality,

$$\angle(-[\mathbf{v}_{ij}]_\times \bar{\mathtt{R}}_{\mathtt{A}_i}\mathbf{u}_{ij}, \bar{\mathbf{t}}_{\mathtt{A}_i}) \le \tfrac{\pi}{2} + \epsilon_{\min} + \gamma_{ij},$$

is almost identical. We just use the fact that

$$\angle(-[\mathbf{v}_{ij}]_\times \bar{\mathtt{R}}_{\mathtt{A}_i}\mathbf{u}_{ij}, -[\mathbf{v}_{ij}]_\times \hat{\mathtt{R}}_{\mathtt{A}_i}\mathbf{u}_{ij}) = \angle([\mathbf{v}_{ij}]_\times \bar{\mathtt{R}}_{\mathtt{A}_i}\mathbf{u}_{ij}, [\mathbf{v}_{ij}]_\times \hat{\mathtt{R}}_{\mathtt{A}_i}\mathbf{u}_{ij}),$$

and the presumption $\angle(-[\mathbf{v}_{ij}]_\times \hat{\mathtt{R}}_{\mathtt{A}_i}\mathbf{u}_{ij}, \hat{\mathbf{t}}_{\mathtt{A}_i}) \le \frac{\pi}{2} + \epsilon_{\min}$.

The proof of the second part of the lemma is analogous to the proof of the second part of Lemma 3 in [4]. □

5.2. A Linear Programming Solution

Lemma 9 justifies the substitution of the hard 6-degrees-of-freedom Problem 3 by 3-degrees-of-freedom Problem 4 as the feasibility test for branch-and-bound algorithm. Albeit easier, Problem 4 is still a non-convex problem. In this section we propose yet another relaxation of Problem 3. This time however, the relaxed problem will be convex and easily decidable by Linear Programming.

Let once again $D_\sigma \subset \mathbb{B}_\pi$ be a cubic block and $\bar{\mathtt{R}}_{\mathtt{X}}$ the rotation represented by the center of the block. In Problem 4, a correspondence $\mathbf{u}_{ij} \leftrightarrow \mathbf{v}_{ij}$ imposes a conic constraint on $\bar{\mathbf{t}}_{\mathtt{A}_i}$ determined by the cone C_{ij} with axis $\mathbf{c}_{ij} = [\mathbf{v}_{ij}]_\times \bar{\mathtt{R}}_{\mathtt{A}_i}\mathbf{u}_{ij}$ and aperture $\alpha_{ij} = \pi - 2(\epsilon_{\min} + \gamma_{ij})$, see Figure 4a. Another correspondence $\mathbf{u}_{ik} \leftrightarrow \mathbf{v}_{ik}$ from the same

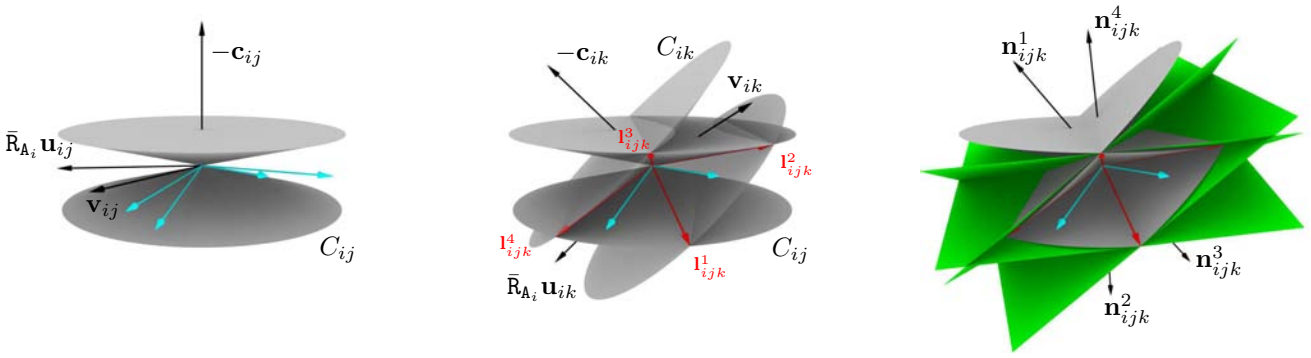

(a) (b) (c)

Figure 4: (a) The conic constraint imposed on $\bar{\mathbf{t}}_{\mathtt{A}_i}$ by the correspondence $\mathbf{u}_{ij} \leftrightarrow \mathbf{v}_{ij}$. The cyan vectors indicate several possible configurations of $\bar{\mathbf{t}}_{\mathtt{A}_i}$. (b) If the apertures α_j, α_k are sufficiently large, cones C_j and C_k intersect in up to four lines $\mathbf{l}^1_{ijk}, \mathbf{l}^2_{ijk}, \mathbf{l}^3_{ijk}, \mathbf{l}^4_{ijk}$. (c) The linear constraints are imposed by correspondences $\mathbf{u}_{ij} \leftrightarrow \mathbf{v}_{ij}$, $\mathbf{u}_{ik} \leftrightarrow \mathbf{v}_{ik}$ and determined by the normals $\mathbf{n}^1_{ijk}, \mathbf{n}^2_{ijk}, \mathbf{n}^3_{ijk}, \mathbf{n}^4_{ijk}$.

i-th motion imposes a different conic constraint, this time determined by the cone C_{ik} with axis $\mathbf{c}_{ik} = [\mathbf{v}_{ik}]_\times \bar{\mathtt{R}}_{\mathtt{A}_i}\mathbf{u}_{ik}$ and aperture $\alpha_{ik} = \pi - 2(\epsilon_{\min} + \gamma_{ik})$.

Now let us consider the mutual configuration of cones C_{ij} and C_{ik}. If the apertures α_{ij}, α_{ik} are sufficiently large, the two cones intersect, see Figure 4b. Since the cones share the same apex, they intersect in up to four lines—generatrices of the both cones—$\mathbf{l}^1_{ijk}$, $\mathbf{l}^2_{ijk}$, $\mathbf{l}^3_{ijk}$, and $\mathbf{l}^4_{ijk}$. These lines form the edges of a pyramid P_{ijk} in which every vector satisfying *both* conic constraints has to lie. The pyramid P_{ijk} has four faces lying in four planes, see Figure 4c. These planes can be determined by their normals $\mathbf{n}^1_{ijk}$, $\mathbf{n}^2_{ijk}$, $\mathbf{n}^3_{ijk}$, and $\mathbf{n}^4_{ijk}$ as

$$\mathbf{n}^1_{ijk} = \left[\mathbf{l}^1_{ijk}\right]_\times \mathbf{l}^2_{ijk}, \;\; \mathbf{n}^2_{ijk} = \left[\mathbf{l}^2_{ijk}\right]_\times \mathbf{l}^3_{ijk},$$
$$\mathbf{n}^3_{ijk} = \left[\mathbf{l}^3_{ijk}\right]_\times \mathbf{l}^4_{ijk}, \;\; \mathbf{n}^4_{ijk} = \left[\mathbf{l}^4_{ijk}\right]_\times \mathbf{l}^1_{ijk}.$$

It is easy to see that every vector $\bar{\mathbf{t}}_{\mathtt{A}_i}$ that satisfies both conical constrains satisfies all of the following linear constraints as well

$$\bar{\mathbf{t}}^\top_{\mathtt{A}_i}\mathbf{n}^1_{ijk} \geq 0,\; \bar{\mathbf{t}}^\top_{\mathtt{A}_i}\mathbf{n}^2_{ijk} \geq 0,\; \bar{\mathbf{t}}^\top_{\mathtt{A}_i}\mathbf{n}^3_{ijk} \geq 0,\; \bar{\mathbf{t}}^\top_{\mathtt{A}_i}\mathbf{n}^4_{ijk} \geq 0. \quad (6)$$

Note that these constraints are also linear in $\mathbf{t}'_{\mathtt{X}}$.

On the other hand, if the apertures α_{ij}, α_{ik} are too small, cones C_{ij} and C_{ik} don't necessarily have to intersect and the conic constraints cannot be replaced by the linear ones. Figure 5 will help us to determine when exactly such a situation arises. Let $C^+_{ij}, C^-_{ij}, C^+_{ik}, C^-_{ik}$ be the nappes of the cones C_{ij}, C_{ik} determined by the vectors $\mathbf{c}_{ij}, -\mathbf{c}_{ij}, \mathbf{c}_{ik}, -\mathbf{c}_{ik}$ respectively. The nappes C^+_{ij}, C^+_{ik} intersect in two line segments $\mathbf{l}^1_{ijk}$ and $-\mathbf{l}^3_{ijk}$ iff

$$\angle(\mathbf{c}_{ij}, \mathbf{c}_{ik}) \;<\; \tfrac{\alpha_{ij}+\alpha_{ik}}{2}. \quad (7)$$

In case of equality of the terms in 7 the nappes are tangential and share only one common generatrix. Analogously,

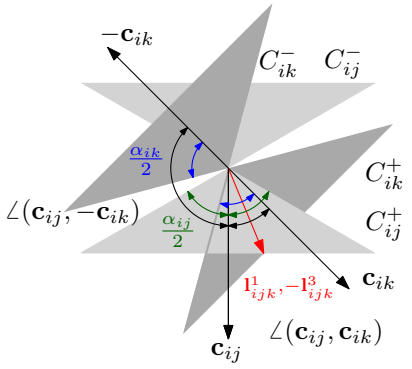

Figure 5: Example configuration of the conic constraints imposed by correspondences $\mathbf{u}_{ij} \leftrightarrow \mathbf{v}_{ij}$ and $\mathbf{u}_{ik} \leftrightarrow \mathbf{v}_{ik}$. Since Inequality 7 holds, the nappes C^+_{ij}, C^+_{ik} intersect in $\mathbf{l}^1_{ijk}$ and $-\mathbf{l}^3_{ijk}$. However, Inequality 8 does not hold and the cones C_{ij}, C_{ik} do not form the pyramid P_{ijk}.

the line segments $\mathbf{l}^2_{ijk}$ and $-\mathbf{l}^4_{ijk}$ are the intersections of the nappes C^+_{ij}, C^-_{ik} iff

$$\angle(\mathbf{c}_{ij}, -\mathbf{c}_{ik}) \;<\; \tfrac{\alpha_{ij}+\alpha_{ik}}{2}. \quad (8)$$

Inequalities 7 and 8 are thus necessary and sufficient conditions for C_{ij}, C_{ik} to form the pyramid P_{ijk}.

Note that the intersection of cones C_{ij} and C_{ik} determines not only the pyramid P_{ijk}, but also a pyramid P'_{ijk} symmetrical to P_{ijk}, with the origin as the point of symmetry. However, since we assumed that the correspondences satisfy the cheirality condition, only constraints relevant to one of the pyramids are applicable. In the following we will assume, without loss of generality, that P_{ijk} forms the applicable constraints. Formulas for lines $\mathbf{l}^1_{ijk}$, $\mathbf{l}^2_{ijk}$, $\mathbf{l}^3_{ijk}$, $\mathbf{l}^4_{ijk}$ can be obtained by using elementary algebra.

Now we can formulate a linear relaxation of Problem 4, which in turn is a non-convex relaxation of Problem 3.

Problem 5

$$\begin{aligned}
&\textit{Given} && D_\sigma, \epsilon_{\min}, \bar{\mathtt{R}}_{\mathtt{X}} \\
&\textit{does there exist} && \mathbf{t}'_{\mathtt{X}} \\
&\textit{subject to} && \bar{\mathbf{t}}_{\mathtt{A}_i}^{\top} \mathbf{n}_{ijk}^1 \geq 0 \\
& && \bar{\mathbf{t}}_{\mathtt{A}_i}^{\top} \mathbf{n}_{ijk}^2 \geq 0 \\
& && \bar{\mathbf{t}}_{\mathtt{A}_i}^{\top} \mathbf{n}_{ijk}^3 \geq 0 \\
& && \bar{\mathbf{t}}_{\mathtt{A}_i}^{\top} \mathbf{n}_{ijk}^4 \geq 0 \\
&\textit{for} && i = 1, \ldots, n,\ j, k = 1, \ldots, m \\
&\textit{such that} && \angle(\pm \mathbf{v}_{ij}, \bar{\mathtt{R}}_{\mathtt{A}} \mathbf{u}_{ij}) > 2 \left\| \boldsymbol{\beta}_i \right\| \sin(\sqrt{3}\sigma/2) \\
&\textit{and} && \textit{Inequalities 7 and 8 hold?}
\end{aligned}$$

An analogy to the formulation of Lemma 9 holds for Problems 4 and 5. Its proof follows from the geometrical construction of the linear constraints as the convex hull of the conic constraints.

6. The Hand-Eye Calibration Algorithm

This section sums up the branch and bound algorithm for hand eye calibration into a more comprehensible pseudo-code form.

First, let us review the hand-eye feasibility test, see Algorithm 1. For every cubic block D_σ the algorithm solves Problem 5. Due to the quite strict assumptions—Lemma 8 and Inequalities 7, 8—not all correspondences produce linear constraints. Indeed, for a large block there might be no feasible correspondences at all. Feasibility of such a block cannot be decided by Problem 5 and it has to be declared feasible by default. However the smaller the blocks get, the more correspondences can produce linear constraints and Problem 5 is more likely to be decidable.

Further, because Problem 5 is a feasibility problem, an LP solver will generally provide a basic feasible solution that does not minimize the nonlinear objective function $\|\mathbf{e}\|_\infty$. In order to speed up the convergence of the algorithm, we use a feasible solution to Problem 5 as an initial estimate for the following non-linear optimization problem:

Problem 6

$$\begin{aligned}
&\textit{Given} && \bar{\mathtt{R}}_{\mathtt{X}} \\
&\textit{minimize} && \|\mathbf{e}\|_2 = \textstyle\sum_{i,j} (\angle([\mathbf{v}_{ij}]_\times \bar{\mathtt{R}}_{\mathtt{A}_i} \mathbf{u}_{ij}, \bar{\mathbf{t}}_{\mathtt{A}_i}) - \frac{\pi}{2})^2 \\
&\textit{for} && i = 1, \ldots, n,\ j, k = 1, \ldots, m \\
&\textit{subject to} && \textit{the initial estimate } \mathbf{t}'_{\mathtt{X}}.
\end{aligned}$$

Since Problem 6 minimizes $\|\mathbf{e}\|_2$, it does not necessarily have to provide a solution with better $\|\mathbf{e}\|_\infty$. However, we observe that it helps to accelerate the overall convergence.

Finally, let us conclude with the branch-and-bound part of the algorithm, see Algorithm 2. The algorithm is initialized by the cubic block $D_\pi = \langle -\pi, \pi \rangle^3$. Such a block is redundant since $\mathbb{B}_\pi \subsetneq \langle -\pi, \pi \rangle^3$, but this fact does not impair the algorithm. Feasible blocks are divided into 8 cubic subblocks and stored in a queue $\mathbf{Q}$, making the algorithm breadth-first search. The search is terminated when the size of the blocks σ reaches a sufficiently small size $\sigma_{\min}$.

Algorithm 1 Feasibility Test

Require: $D, \epsilon_{\min} > 0$
  $\bar{\mathtt{R}}_{\mathtt{X}} \leftarrow$ rotation represented by the center of cube D
  $\sigma \leftarrow$ half-side length of D
  $\mathbf{L} \leftarrow \emptyset$
  for $i = 1$ **to** number of motions **do**

    // Collect feasible correspondences s.t. Lemma 8
    $\mathbf{C}_i \leftarrow \emptyset$
    for $j = 1$ **to** number of correspondences **do**
      if $\angle(\pm \mathbf{v}_{ij}, \bar{\mathtt{R}}_{\mathtt{A}} \mathbf{u}_{ij}) > 2 \left\| \boldsymbol{\beta}_i \right\| \sin(\sqrt{3}\sigma/2)$ **then**
        $\mathbf{C}_i \leftarrow \mathbf{C}_i \cup \{j\}$
      end if
    end for

    // Collect linear constraints s.t. Inequalities 7 and 8
    while $\mathbf{C}_i \neq \emptyset$ **do**
      $j, k \in \mathbf{C}_i$
      if $\angle(\mathbf{c}_{ij}, \pm \mathbf{c}_{ik}) < (\alpha_{ij} + \alpha_{ik})/2$ **then**
        $\mathbf{L} \leftarrow \mathbf{L} \cup \{\langle i, \mathbf{n}_{ijk}^1 \rangle, \langle i, \mathbf{n}_{ijk}^2 \rangle, \langle i, \mathbf{n}_{ijk}^3 \rangle, \langle i, \mathbf{n}_{ijk}^4 \rangle\}$
        $\mathbf{C}_i \leftarrow \mathbf{C}_i \setminus \{j, k\}$
      end if
    end while

  end for

  if $\mathbf{L} \equiv \emptyset$ **then**
    feasible $\leftarrow 1$
    return $\{$*feasible*$\}$
  end if

  // Solve Problem 5
  $\mathbf{t}'_{\mathtt{X}} \leftarrow \mathbf{t}'_{\mathtt{X}}$ such that $\forall \langle i, \mathbf{n} \rangle \in \mathbf{L} \colon \bar{\mathbf{t}}_{\mathtt{A}_i}^{\top} \mathbf{n} \geq 0$
  if such a $\mathbf{t}'_{\mathtt{X}}$ does not exist **then**
    feasible $\leftarrow 0$
    return $\{$*feasible*$\}$
  else
    feasible $\leftarrow 1$
    $\epsilon \leftarrow \max_{i,j} |\angle([\mathbf{v}_{ij}]_\times \bar{\mathtt{R}}_{\mathtt{A}_i} \mathbf{u}_{ij}, \bar{\mathbf{t}}_{\mathtt{A}_i}) - \frac{\pi}{2}|$
  end if

  // Solve Problem 6
  $\tilde{\mathbf{t}}'_{\mathtt{X}} \leftarrow \min_{\mathbf{t}'_{\mathtt{X}}} \sum_{i,j} \left(\angle([\mathbf{v}_{ij}]_\times \bar{\mathtt{R}}_{\mathtt{A}_i} \mathbf{u}_{ij}, \bar{\mathbf{t}}_{\mathtt{A}_i}) - \frac{\pi}{2} \right)^2$
  $\tilde{\epsilon} \leftarrow \max_{i,j} |\angle([\mathbf{v}_{ij}]_\times \bar{\mathtt{R}}_{\mathtt{A}_i} \mathbf{u}_{ij}, \bar{\mathbf{t}}_{\mathtt{A}_i}(\tilde{\mathbf{t}}'_{\mathtt{X}})) - \frac{\pi}{2}|$
  if $\tilde{\epsilon} < \epsilon$ **then**
    $\epsilon \leftarrow \tilde{\epsilon}$
    $\mathbf{t}'_{\mathtt{X}} \leftarrow \tilde{\mathbf{t}}'_{\mathtt{X}}$
  end if

  return $\{$*feasible*$, \epsilon, \bar{\mathtt{R}}_{\mathtt{X}}, \mathbf{t}'_{\mathtt{X}}\}$

Algorithm 2 Branch and Bound

Require: initial estimate of $\epsilon_{\min}$, stopping criterion $\sigma_{\min}$
  $D_\pi \leftarrow \langle -\pi, \pi \rangle^3$
  PushBack($\mathbf{Q}, D_\pi$)
  $\sigma \leftarrow 2\pi$
  while $\sigma > \sigma_{\min}$ **do**
    $D \leftarrow$ PopFront($\mathbf{Q}$)
    $\sigma \leftarrow$ half-side length of D
    $\{\mathit{feasible}, \epsilon, \bar{\mathtt{R}}_\mathtt{X}, \mathbf{t}'_\mathtt{X}\} \leftarrow$ FeasibilityTest($D, \epsilon_{\min}$)
    if $\mathit{feasible} \equiv$ **true then**
      if $\epsilon < \epsilon_{\min}$ **then**
        $\hat{\mathtt{R}}_\mathtt{X} \leftarrow \bar{\mathtt{R}}_\mathtt{X}$
        $\hat{\mathbf{t}}'_\mathtt{X} \leftarrow \mathbf{t}'_\mathtt{X}$
        $\epsilon_{\min} \leftarrow \epsilon$
      end if
      PushBack($\mathbf{Q}$, SubdivideBlock(D))
    end if
  end while
  $\hat{\mathbf{t}}_\mathtt{X} \leftarrow -\hat{\mathtt{R}}_\mathtt{X}\hat{\mathbf{t}}'_\mathtt{X}$
  return $\{\hat{\mathtt{R}}_\mathtt{X}, \hat{\mathbf{t}}_\mathtt{X}, \epsilon_{\min}\}$

7. Experimental Results

Next, the performance of the proposed algorithm is evaluated using both synthetically generated and real world data measurements. We use GLPK [1] to solve Problem 5 and levmar [8] to solve nonlinear Problem 6. The values of the initial estimate $\epsilon_{\min}$ and the stopping criterion $\sigma_{\min}$ were set to 0.02 and 0.0005 respectively. All the reported times were achieved on a 3GHz Intel Core i7 based desktop computer running 64-bit Linux. The source code is available at `http://cmp.felk.cvut.cz/~hellej1/bbhec/`.

7.1. Experiment with Synthetic Data

A synthetic scene consisting of 100 3D points was generated into a ball of radius 1,000 mm. 10 absolute camera poses were set up so that (i) the centers of the cameras were outside the ball but close to its 'surface', (ii) the centers were positioned so that the offsets of the camera motions would be ~500 mm and (iii) the cameras faced approximately the center of the ball. In order to simulate the effect of decreasing field of view (FOV), 7 progressively smaller balls were generated inside the initial ball so that the balls shared the centers and the volume of the newly created ball was half the volume of the previous ball. This defined 8 FOV levels, namely 180°, 105°, 78°, 60°, 47°, 37°, 29°, and 23°. Additional 3D points were generated inside each of the smaller balls in order to have exactly 100 3D points at each FOV level measured in the respective cameras giving raise to correspondences $\mathbf{u}_{ij} \leftrightarrow \mathbf{v}_{ij}$ (newly generated points did not contribute to the larger balls).

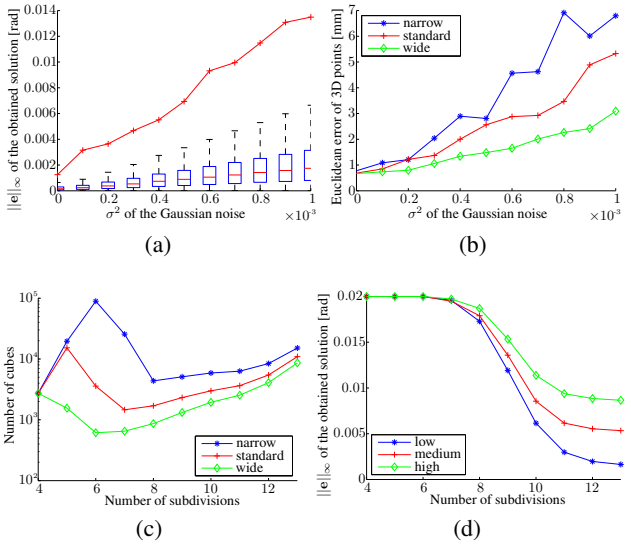

Figure 6: *Synthetic data experiment.* (a) The maximum residual error of the obtained solutions for the various values of σ^2(red line) and the distribution of the measured errors over all correspondences (boxes). (b) The mean Euclidean distance between the 3D points transformed to the gripper's coordinate systems using ground truth $\mathtt{X}$ and the 3D points transformed to the gripper's coordinate systems using the estimated $\mathtt{X}$. Different FOV levels were clustered into three groups. (c) The mean number of remaining cubes plotted against the number of subdivision phases. Note that the computation starts after the fourth subdivision. (d) The mean residual error at the beginning of the respective subdivision phase. Different noise levels were clustered into three groups.

Further, ten random transformations $\mathtt{X}$ were generated and the optimization tasks composed of the known correspondences $\mathbf{u}_{ij} \leftrightarrow \mathbf{v}_{ij}$ and 9 motions $\mathtt{B}_i$—computed from the known absolute camera poses and the generated $\mathtt{X}$—were constructed for each of the 8 FOV levels. Finally, the correspondences were corrupted with Gaussian noise in the angular domain using 11 noise levels, $\sigma^2 \in \langle 0, 10^{-3} \rangle$ in 10^{-4} steps resulting to 88 tasks per transformation.

The results of the experiment are shown in Figure 6. Note that the median of the measured errors over all correspondences is approximately one order of magnitude smaller than the maximum residual error. The actual errors of the calibration—being the Euclidean distance between the 3D points transformed to the gripper's coordinate systems using ground truth $\mathtt{X}$ and the 3D points transformed to the gripper's coordinate systems using the estimated $\mathtt{X}$—are lower for wide FOV. Considering the timings resulting from both single-threaded and multi-threaded C++ implementations of the algorithm,

	narrow FOV	standard FOV	wide FOV
1 thread	1985.5 s	792.7 s	478.7 s
8 threads	430.4 s	168.0 s	101.5 s

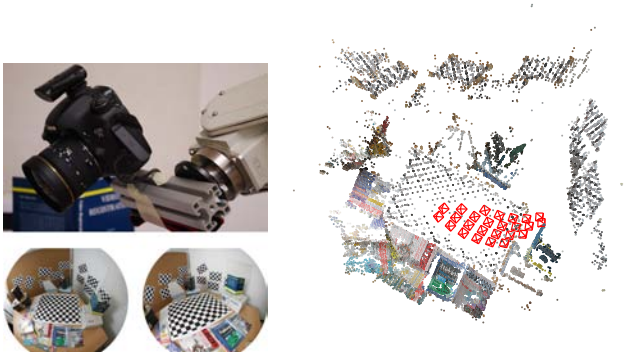

(a) (b)

Figure 7: *Real data experiment*. (a) Close up of the camera-gripper rig, sample images from the sequence. (b) Model resulting from SfM, cameras are denoted by red pyramids.

the solutions are found faster for wide FOV as the correspondences of narrow FOV camera pairs do not generate enough linear constraints for large blocks and thus more blocks are subdivided.

7.2. Experiment with Real Data

A Mitsubishi MELFA-RV-6S serial manipulator with a Canon 7D digital SLR camera and a Sigma 8 mm lens (pixel size ~0.0011 rad, FOV ~130°) were used to acquire the data for the real experiment. The robot was instructed to move the gripper along the surface of a sphere of radius ~700 mm centered in the middle of the scene objects. The position of the gripper was adjusted using the yaw and pitch angles measured from the center of the sphere to reach 25 different locations at four different pitch angles and the gripper was set to face the center of the sphere, see Figure 7a.

The internal calibration of the camera was obtained from several images of a checkerboard using OCamCalib [9] as a polynomial model of degree 3. A state-of-the-art sequential SfM software [12] was used to automatically generate image feature points, match them, verify the matches by pairwise epipolar geometries, and create tracks and triangulated 3D points, see Figure 7b. We used 24 motions $\mathtt{B}_i$ and 100 correspondences $\mathbf{u}_{ij} \leftrightarrow \mathbf{v}_{ij}$ per motion—randomly selected from the feature tracks—to construct the optimization task. Note that the knowledge of the relative camera poses $\mathtt{A}_i$ and the triangulated 3D points was not used.

We executed the task for $\epsilon_{\min}$ being 0.1 and received a solution with residual error $\|\mathbf{e}\|_\infty = 0.0414$ rad (median of the measured errors 0.0055 rad) in 1572.8 seconds (running in 8 threads). The computed rotation $\mathtt{R}_\mathtt{X}$ was close to the rotation along the z-axis by $\pi/4$ as expected.

8. Conclusion

In this paper we removed the requirement for known camera extrinsics from hand-eye calibration problem. Since the presented algorithm is completely independent on the scene geometry and scale, there is no need for a known calibration device and the calibration can be performed solely from a general scene. The algorithm solves for both the unknown rotation and translation simultaneously and is guaranteed to be globally optimal with respect to L_∞-norm.

Acknowledgment The authors were supported by the EC under projects FP7-SPACE-218814 PRoVisG and FP7-SPACE-241523 PRoViScout and by Grant Agency of the CTU Prague project SGS10/277/OHK3/3T/13. The authors would also like to thank Martin Meloun for his help with the real-data experiment.

References

[1] GNU linear programming kit version 4.47, 2011, `http://www.gnu.org/software/glpk/glpk.html`

[2] J. C. K. Chou and M. Kamel. Finding the position and orientation of a sensor on a robot manipulator using quaternions. *IJRR*, 10(3):240–254, 1991.

[3] K. Daniilidis. Hand-eye calibration using dual quaternions. *IJRR*, 18:286–298, 1998.

[4] R. Hartley and F. Kahl. Global optimization through rotation space search. *IJCV*, 82(1):64–79, 2009.

[5] R. Hartley and A. Zisserman. *Multiple View Geometry in Computer Vision*. Cambridge University Press, 2003.

[6] J. Heller, M. Havlena, A. Sugimoto, and T. Pajdla. Structure-from-motion based hand-eye calibration using L_∞ minimization. In *CVPR*, pp. 3497–3503, 2011.

[7] R. Horaud and F. Dornaika. Hand-eye calibration. *IJRR*, 14(3):195–210, 1995.

[8] M. Lourakis. levmar: Levenberg-marquardt non-linear least squares algorithms in C/C++, 2004, `http://www.ics.forth.gr/~lourakis/levmar/`

[9] D. Scaramuzza, A. Martinelli, and R. Siegwart. A toolbox for easily calibrating omnidirectional cameras. In *International Conference on Intelligent Robots and Systems*, pp. 5695–5701, 2006.

[10] Y. Seo, Y.-J. Choi, and S. W. Lee. A branch-and-bound algorithm for globally optimal calibration of a camera-and-rotation-sensor system. In *ICCV*, pp. 1173–1178, 2009.

[11] Y. Shiu and S. Ahmad. Calibration of wrist-mounted robotic sensors by solving homogeneous transform equations of the form AX=XB. *IEEE Transactions on Robotics and Automation*, 5(1):16–29, 1989.

[12] A. Torii, M. Havlena, and T. Pajdla. Omnidirectional image stabilization for visual object recognition. *IJCV*, 91(2):157–174, 2011.

[13] R. Tsai and R. Lenz. Real time versatile robotics hand/eye calibration using 3d machine vision. In *International Conference on Robotics and Automation*, pp. 554–561 vol.1, 1988.

[14] R. Tsai and R. Lenz. A new technique for fully autonomous and efficient 3d robotics hand/eye calibration. *IEEE Transactions on Robotics and Automation*, 5(3):345–358, 1989.

[15] H. Zhang. Hand/eye calibration for electronic assembly robots. *IEEE Transactions on Robotics and Automation*, 14(4):612–616, 1998.